Giant slip lengths of a simple fluid at vibrating solid interfaces

Aurélien Drezet,[1] Alessandro Siria,[1,2] Serge Huant,[1] and Joël Chevrier[1]
[1]*Institut Néel, CNRS and Université Joseph Fourier Grenoble, BP 166, 38042 Grenoble Cedex 9, France*
[2]*CEA/LETI-MINATEC, 17 Avenue des Martyrs, 38054 Grenoble Cedex 9, France*
(Received 13 January 2010; published 23 April 2010)

It has been shown recently [A. Siria, A. Drezet, F. Marchi, F. Comin, S. Huant, and J. Chevrier, Phys. Rev. Lett. **102**, 254503 (2009)] that in the plane-plane configuration, a mechanical resonator vibrating close to a rigid wall in a simple fluid can be overdamped to a frozen regime. Here, by solving analytically the Navier-Stokes equations with partial slip boundary conditions at the solid-fluid interface, we develop a theoretical approach justifying and extending these earlier findings. We show in particular that in the perfect-slip regime, the abovementioned results are, in the plane-plane configuration, very general and robust with respect to lever geometry considerations. We compare the results to those obtained previously for the sphere moving perpendicularly and close to a plane in a simple fluid and discuss in more details the differences concerning the dependence of the friction forces with the gap distance separating the moving object (i.e., plane or sphere) from the fixed plane. We show that the plane-plane geometry is more sensitive than the sphere-plane geometry for the measurement of slippage coefficients. Finally, we show that the submicron fluidic effect reported in the reference above, and discussed further in the present work, can have dramatic implications in the design of nanoelectromechanical systems.

DOI: 10.1103/PhysRevE.81.046315 PACS number(s): 47.61.Fg, 47.15.Rq, 85.85.+j, 07.79.Lh

I. INTRODUCTION

Nanomechanical resonators and nanoelectromechanical systems are widely used in a multitude of applications such as ultrafast actuation and sensing at the zeptogram and sub-atto-Newton scales [1–5]. The extraordinary sensitivity that such nanoelectromechanical systems (NEMSs) provide relies mainly on their very high oscillating pulsations and quality factors Q. However, while Q factors in the tens or hundreds of thousands can be obtained in vacuum and/or cryogenic environments, these values degrade dramatically in liquid and gas phases meaning that much more work is still to be done to reach the technological level (see, however, [3,6]). It is therefore necessary to characterize more precisely the viscous forces exerted by fluids on the vibrating motion of NEMS and this constitutes the motivation for the present work.

Over the last years, micro- and nanofluidics experiments [7] reported that the physical properties of fluids flowing into or around confined systems, such as nanochannels [8], are strongly modified compared to those encountered at the micro- and macroscales. In particular, it has been shown that the usual no-slip boundary conditions, which are universally used since the 19th century to model the behavior of Newtonian fluids at a solid interface, break down at the nanoscale [9]. Such modifications of boundary conditions are also expected to have a huge impact on NEMS dynamics since properties known for microelectromechanical systems (MEMSs) [10–15] cannot simply be scaled down to the nanorealm.

In a recent work, we investigated the importance of gas damping on a thermally actuated microlever as it is gradually approached toward an infinite wall in parallel geometry [16]. The experiment performed at room temperature in air showed that the sub-Angstrom lever oscillation amplitude, i.e., in the direction perpendicular to the parallel planes, is completely frozen as the gap d is progressively decreased from 20 μm to 400 nm. Moreover, the friction force recorded was much larger than that predicted by the Navier-Stokes hydrodynamical equations solved together with the no-slip boundary conditions. Instead, the reported results are qualitatively and quantitatively well understood if one accepts the perfect-slip boundary conditions for which friction at the lever-gas interface is prohibited.

The aim of the present paper is twofold. First, we study theoretically the motion of the Newtonian fluid, i.e., air, around the oscillating micro plate. Starting with the linearized Navier-Stokes equation, we analytically show that perfect-slip boundary conditions lead to the correct dynamical behavior reported experimentally in Ref. [16]. We compare our findings to other more traditional approaches based on the no-slip boundary conditions and show that they necessarily conflict with the experimental facts. During the analysis, we also discuss the different possible boundary conditions and in particular the impact of the slip length of the beam dynamical behavior. The second goal of this paper is to show the important implications that our findings may have on the engineering and architecture of future NEMSs operating in gaseous environment. Here, on the basis of the results obtained in Ref. [16] for a model system, we discuss precisely the existence of a critical overdamped regime for NEMS oscillating in fluids and study the influence of materials, and geometrical and intrinsic dynamical properties on this regime.

The paper is organized as follows. In Sec. II, we discuss the general characteristics of the dynamic problem in conjunction with Navier-Stokes equations and boundary conditions. In Sec. III, the static regime corresponding to various slip lengths and valid for small gap values is studied analytically and compared (successfully) to the experimental results reported in Ref. [16]. In Sec. IV, we briefly discuss the possible microscopic mechanisms involved in order to explain the reported results. In particular, we compare the calculations obtained here for the plane-plane geometry to those already obtained in the sphere-plane configuration by Taylor and Vinogradova [17,18]. We then show that the plane-plane

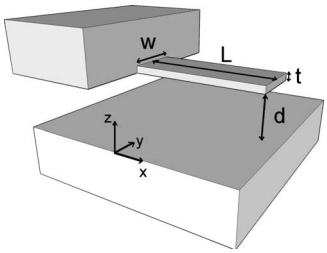

FIG. 1. Scheme of the one end-clamped parallelepiped cantilever used in Ref. [16]. The lever has dimensions t, L, and w and is vibrating in the z direction at a distance d from the substrate.

geometry (i) constitutes the ideal candidate to measure slippage coefficients on a large range of d values and (ii) is more sensitive than the usual sphere-plane geometry. Finally, in Sec. V, we discuss the consequences of our findings for NEMS dynamics. A summary is given in Sec. VI.

II. MECHANICAL OSCILLATOR IN A NEWTONIAN FLUID

We consider a thin silicon commercial cantilever used in atomic force microscopy (AFM) for liquid imaging [16]. This system is modeled as a parallelepiped with length L, width w, and thickness t. The lever is clamped by one end and oscillates mainly along the z direction (see Fig. 1). In vacuum, this beam may be viewed as a harmonic oscillator with an intrinsic resonance pulsation ω_0 and effective mass m (internal losses can be fairly neglected in the following analysis). In the fluid, the viscous force acting on the lever is characterized by a dissipative coefficient γ connecting the viscous force F_z normal to the lever to the velocity U of the lever along the same direction: $F_z=-\gamma U$. At short distance, i.e., in the nonretarded regime, γ is given by [16]

$$\gamma = \frac{2\eta L w}{d}, \tag{1}$$

where η is the (dynamic) fluid viscosity and d the distance between the lever and the substrate (see Fig. 1). As we will now show, this law results directly from the perfect-slip boundary conditions applied to the Navier-Stokes equation and it differs from the usual $\gamma \simeq \eta w L^3/d^3$ behavior deduced by considering the no slip conditions [16,19].

To derive this result, we start from the nonlinear Navier-Stokes equations for an incompressible fluid

$$\rho[\partial_t \vec{v} + (\vec{v}\cdot\vec{\nabla})\vec{v}] = \eta\vec{\nabla}^2\vec{v} - \vec{\nabla}p, \tag{2}$$

where $\vec{v}$ is the local fluid velocity, ρ its density, and p the gas pressure. To calculate the gas flow around the lever, we take into account specific properties of the system under study. First, the importance of the nonlinear term $(\vec{v}\cdot\vec{\nabla})\vec{v}$ can be estimated from the knowledge of the Reynolds number $R_e := vX/\nu = \rho v X/\eta$ calculated for a characteristic length X and fluid velocity v ($\nu = \eta/\rho = 1.5\times10^{-5}$ m^2/s is the kinematic viscosity). In the present context, a correct order of magnitude of the velocity in the fluid is given by the lever velocity components U_x, $U_z := U$ along the x and z directions, respectively. An important related feature is that we have here $U_x \ll U$. Indeed, writing $\theta \simeq \delta z/L$ (with $\delta z = 0.05$ nm the typical lever oscillation amplitude), the main angle shown by the lever with the x axis, we get the estimation $U_x/U \simeq \theta \simeq 10^{-6}$ which implies that the motion is mainly vertical. To simplify our analysis, we therefore assume that the lever is a horizontal plate vibrating along the z direction. The lever oscillating at the frequency $\omega/(2\pi) = 50$ kHz, one obtains $U \simeq \omega\delta z/(2\pi) \simeq 2.5\times10^{-6}$ m/s, and thus with $X := d = 50$ μm,

$$R_e = \frac{\omega \delta z d}{2\pi\nu} \simeq 0.8\times10^{-5} \ll 1. \tag{3}$$

As a consequence of this ultrasmall Reynolds number, we will completely neglect nonlinearity in the rest of this work. As a corollary of this analysis, we also deduce the Mach number $M = v/c \sim U/c \simeq 10^{-8} \ll 1$ (c sound velocity in air). The vanishing value of M justifies the fluid incompressibility hypothesis $\vec{\nabla}\cdot\vec{v} = 0$.

The second question that we should deal with concerns the amplitude of the dynamical term $\rho\partial_t\vec{v} = -i\omega_0\rho\vec{v}$ in Eq. (2). Since we are concerned with harmonic oscillations, we introduce a second Reynolds number

$$R_e' = \frac{\omega_0 d^2}{\nu} \simeq 2\times10^{-2}(d[\mu\text{m}])^2, \tag{4}$$

where $d[\mu\text{m}]$ is the measure of d in micrometers. Clearly R_e' (and therefore $\rho\partial_t\vec{v}$) is negligible as far as $d \ll \sqrt{2\nu/\omega_0} \simeq 10$ μm, i.e., as far as the gap d is smaller than the boundary layer thickness δ_B (see below for discussion). In the present work, we will only consider this static regime and neglect the dynamic term.

In order to solve the linearized Navier-Stokes equation

$$\eta\vec{\nabla}^2\vec{v} - \vec{\nabla}p \simeq 0, \tag{5}$$

one must provide the precise boundary conditions for the fluid velocity at the solid interfaces. The condition for the normal component of the velocity is quite obvious [19,20]. Indeed, since the fluid cannot go through a solid interface, the fluid velocity v_z must equal the velocity of the plate U at $z=d$ and must also vanish along the surface $z=0$ [19,20]. However, the precise form of the conditions for the tangential components v_x and v_y is not so natural and is a subject of debates and controversies since the birth of hydrodynamics [9,21–23]. The problem was already well addressed by Navier [24] who introduced the two most known possibilities which are, respectively, the no-slip and perfect-slip boundary conditions. Following the no-slip hypothesis, the fluid velocity along the interface must equal the in-plane velocity of the solid boundary. In the present case, the no-slip conditions lead to $v_x = v_y = 0$ along the substrate plane $z=0$ and $v_x = U_x \simeq 0$, and $v_y = 0$ along the cantilever interface at $z=d$. The no-slip hypothesis is well documented in the literature and experimentally justified at the macroscale [9,21–23]. It leads however to increasing difficulties and contradictions in the micro- and nanofluidic regimes where fundamental and statistical properties of molecules such as the mean-free path and the surface roughness cannot be ignored [7,9,21–23].

The second extreme possibility, the perfect-slip boundary conditions, supposes having $\partial_z v_i=0$ (from now on we use the notation $i=x,y$) along the solid interface. These are reminiscent for conditions on the viscous stress tensor $\sigma_{iz}=\eta(\partial_z v_i+\partial_i v_z)=0$, meaning that no tangential friction is allowed between fluid and solid. We however point out that the equivalence between the relations $\sigma_{iz}=0$ and $\partial_z v_i=0$ assumes the additional conditions $\partial_i v_z=0$ which implies that v_z does not depend on x,y in the vicinity of the solid boundary (this is obviously true on the interface provided that the boundary conditions on v_z are fulfilled). Beyond these two extreme cases, more realistic approaches were proposed to take into account a possible partial slip at the boundary. In particular, Navier [7,9,21–24] suggested the existence of a surface friction force law $\sigma_{iz}n_z=\kappa v_i$, where $\vec{n}=n_z\hat{z}$ is a unit vector normal to the surface and oriented outwardly from the solid to the fluid and κ a dissipative coefficient. With the same assumptions as before, this leads to

$$n_z\partial_z v_i=\kappa v_i/\eta=v_i/b, \tag{6}$$

where b is the so-called slip length. This law has been considerably studied in the recent years with the advent of micro- and nanofluidics [7,9,22,23]. Equation (6) has been confirmed many times in particular for liquid flows in nanochannels [22]. However, the measurements of the associated slip length b reveal a broad spectrum of values which specifically depend on the system considered [7,23]. This shows that only a microscopic analysis could lead to a better understanding of the phenomenon. Keeping this point for latter discussions, we will here apply the law given by Eq. (6) to our problem and see how it compares to the experimental results.

III. STATIC LIMIT

In the present analysis, we consider the static regime valid for $d\ll\delta_B:=\sqrt{2\nu/\omega_0}$. We must therefore solve the system of coupled equations $\eta\vec{\nabla}^2\vec{v}=\vec{\nabla}p$, $\vec{\nabla}\cdot\vec{v}=0$ together with the conditions given by Eq. (6). The problem is reminiscent for the one solved by Reynolds in the case of two parallel disks in a dissipative fluid. Reynolds considered two disks approaching each other with a constant velocity $\pm U$ along their common axis of symmetry. However, despite geometry differences, Reynolds considered specifically the case of no-slip boundary conditions (which were universally accepted at that time) and not the more general Eq. (6). Using the same approximations than Reynolds, we here suppose $\partial_x v_i,\partial_y v_i\ll\partial_z v_i$, $\partial_x v_z,\partial_y v_z\ll\partial_z v_z$, and $\partial_z p\simeq 0$ which are standard in lubrication theory. We then have

$$\eta\partial_z^2 v_i\simeq\partial_i p. \tag{7}$$

After integration with respect to z, this leads to

$$v_i(x,y,z)=\frac{1}{2\eta}\partial_i p(x,y)z^2+\alpha_i(x,y)z+\beta_i(x,y). \tag{8}$$

To be general, we are introducing two *a priori* different slip lengths b_0 and b_1 for the interfaces at $z=0$ and $z=d$, respectively. This hypothesis implies

$$v_i(z=0)=b_0\partial_z v_i(z=0),\quad v_i(z=d)=-b_1\partial_z v_i(z=d)$$

and therefore

$$v_i(x,y,z)=\frac{1}{2\eta}\partial_i p(x,y)\left[z^2-d\frac{2b_1+d}{b_0+b_1+d}(z+b_0)\right]. \tag{9}$$

The fluid incompressibility relation $\partial_x v_x+\partial_y v_y+\partial_z v_z=0$ and the boundary conditions for v_z at $z=0$ give the expression $v_z(x,y,z)=-\int_0^z(\partial_x v_x+\partial_y v_y)dz$, i.e.,

$$v_z=\frac{1}{2\eta}(\partial_x^2+\partial_y^2)p(x,y)\left[d\frac{2b_1+d}{b_0+b_1+d}\left(\frac{z^2}{2}+b_0 z\right)-\frac{z^3}{3}\right]. \tag{10}$$

At $z=d$, we have the boundary condition $v_z=U$ and we deduce

$$(\partial_x^2+\partial_y^2)p(x,y)=\frac{2\eta U}{\left[\left(-\frac{1}{3}+\frac{1}{2}\frac{2b_1+d}{b_0+b_1+d}\right)d^3+\frac{2b_1+d}{b_0+b_1+d}b_0d^2\right]} \tag{11}$$

and

$$v_z(x,y,z)=\frac{U\left[-\frac{z^3}{3}+d\frac{2b_1+d}{b_0+b_1+d}\left(\frac{z^2}{2}+b_0z\right)\right]}{\left[\left(-\frac{1}{3}+\frac{1}{2}\frac{2b_1+d}{b_0+b_1+d}\right)d^3+\frac{2b_1+d}{b_0+b_1+d}b_0d^2\right]}. \tag{12}$$

In particular, in the limit $b_0=b_1\to+\infty$, we have $v_z=Uz/d$ whereas for $b_0=b_1=0$ we obtain $v_z=6U(-z^3/3+z^2d/2)/d^3$. It should be observed that the solution for v_z in the perfect-slip limit looks like the well-known solution of the Couette problem [19,20] for the permanent fluid motion between two plates in relative and uniform motions along the x direction. It is worth noting that the directions of the fluid motion and the boundary conditions used are however completely different in these two problems (indeed, in the Couette problem, we assume the no-slip boundary conditions and neglect v_z [19,20]). Here, due to the presence of terms with v_z, our approach deviates from this standard result.

The normal force exerted by the fluid located between $z=0$ and $z=d$ on each surface element $dxdy$ of the lever is given by

$$dF_z=[-\sigma_{zz}+p]|_{z=d}dxdy=[-2\eta\partial_z v_z|_{z=d}+p(x)]dxdy, \tag{13}$$

where $\sigma_{zz}=2\eta\partial_z v_z$ is the fluid stress tensor along the z direction and therefore $-\sigma_{zz}|_{z=d}dxdy$ is the dissipative part of the resulting force dF_z. Using Eq. (12), we obtain

$$-\sigma_{zz}|_{z=d} = \frac{2\eta U\left[d^2 - \frac{2b_1+d}{b_0+b_1+d}(d^2+b_0 d)\right]}{\left[\left(-\frac{1}{3}+\frac{1}{2}\frac{2b_1+d}{b_0+b_1+d}\right)d^3 + \frac{2b_1+d}{b_0+b_1+d}b_0 d^2\right]}. \tag{14}$$

Interestingly, this contribution is independent of x,y and of the lateral boundary shape (C) associated with the lever and the substrate. The resulting dissipative force $-\int_{(S)}\sigma_{zz}|_{z=d}dxdy$ on the plate of surface S is consequently

$$F_z^{\text{dissip.}} = \frac{2\eta SU\left[d^2 - \frac{2b_1+d}{b_0+b_1+d}(d^2+b_0 d)\right]}{\left[\left(-\frac{1}{3}+\frac{1}{2}\frac{2b_1+d}{b_0+b_1+d}\right)d^3 + \frac{2b_1+d}{b_0+b_1+d}b_0 d^2\right]}. \tag{15}$$

The second contribution to the force is associated with the volume pressure $p(x,y)$ that is solution of the two-dimensional (2D) Poisson equation $(\partial_x^2+\partial_y^2)p(x,y)=A$, where A is a constant [see Eq. (11)]. Lateral boundary conditions along (C) are here playing explicitly a role in the analysis. Let us suppose, for example, that the substrate is infinitely extended in the $z=0$ plane and that the lever is delimited by a rectangular boundary of length L and width w in the $z=d$ plane. A lengthy Fourier analysis (see the Appendix) shows that the pressure field can be expanded as

$$p(x,y) = p_0 + \frac{4AL^2}{\pi^3}\sum_n \frac{1}{n^3}\sin(\pi n x/L) \times[\alpha_n e^{+\pi n y/L} + \beta_n e^{-\pi n y/L} - 1], \tag{16}$$

where n are odd integers and α_n,β_n are constant coefficients (see the Appendix). To obtain this formula, the boundary condition $p=p_0$ (p_0 is the atmospheric pressure) was imposed on the rectangular contour. Similarly, if we consider the one-dimensional (1D) problem with L finite, $w=+\infty$, and with p a function of x only, we deduce after a direct integration

$$p(x) = p_0 + \frac{A}{2}(x^2 - xL), \tag{17}$$

where we used the boundary conditions $p(0)=p(L)=p_0$. Equivalently, this result could also be obtained from the Fourier expansion $p(x)=p_0-\frac{4AL^2}{\pi^3}\Sigma_n\frac{1}{n^3}\sin(\pi n x/L)$. Finally, as a last example, we consider the circular plate of radius R. Assuming the radial symmetry, this problem leads to the solution

$$p(r) = p_0 + \frac{A}{4}(r^2 - R^2), \tag{18}$$

where r is the radial coordinate and $p(R)=p_0$ along the circular contour of radius R. More generally, by using the uniqueness theorem, it is easily shown that the pressure $p(x,y)$ can always be written as

$$p(x,y) = p_0 + Ag(x,y), \tag{19}$$

where $g(x,y)$ is the solution of $(\partial_x^2+\partial_y^2)g(x,y)=1$ which is univocally determined by the boundary condition $g(x,y)=0$ along the contour. The resulting vertical force due to the pressure field on the plate of surface S is thus given by

$$F_z^{\text{pressure}} = \int\int_{(S)}(p(x,y)-p_0)dxdy = A\int\int_{(S)} g(x,y)dxdy = AS\langle g\rangle, \tag{20}$$

where the term $-p_0$ equilibrating the pressure $+p_0$ from Eq. (19) is due to the force exerted by the fluid on the second side of the cantilever. Considering the examples quoted previously, we find explicitly

$$F_z^{\text{pressure}} = -\frac{8AL^3 w}{\pi^4}\sum_n \frac{1}{n^4}\left[1 - \frac{2L}{\pi n w}\frac{(e^{+\pi n w/(2L)} - e^{-\pi n w/(2L)})^2}{e^{+\pi n w/L} - e^{-\pi n w/L}}\right] \tag{21}$$

for the rectangular plate and

$$F_z^{\text{pressure}} = -\frac{8AL^3 w}{\pi^4}\sum_n \frac{1}{n^4} = -\frac{AL^3 w}{12} \tag{22}$$

for the 1D plate [note that w is a finite width in the y direction introduced for reasons of dimensionality and that Eq. (22) is the limit of Eq. (21) for $w\to+\infty$]. Similarly, for the disk, we deduce

$$F_z^{\text{pressure}} = -\frac{\pi A R^4}{8}. \tag{23}$$

These forces due to pressure can be compared to the dissipative contribution given by Eq. (15) which can equivalently be expressed as

$$F_z^{\text{dissip.}} = AS\left[d^2 - \frac{2b_1+d}{b_0+b_1+d}(d^2+b_0 d)\right] \tag{24}$$

and leads to the total force $F_z=F_z^{\text{pressure}}+F_z^{\text{dissip.}}$,

$$F_z = AS\left[\langle g\rangle + d^2 - \frac{2b_1+d}{b_0+b_1+d}(d^2+b_0 d)\right], \tag{25}$$

with

$$A = \frac{2\eta U}{\left[\left(-\frac{1}{3}+\frac{1}{2}\frac{2b_1+d}{b_0+b_1+d}\right)d^3 + \frac{2b_1+d}{b_0+b_1+d}b_0 d^2\right]}. \tag{26}$$

In the usual limit of vanishing slip lengths, $F_z^{\text{dissip.}}=0$ and we therefore have

$$F_z = \frac{12\eta US\langle g\rangle}{d^3}, \tag{27}$$

which is the generalization of the Reynolds formula for an arbitrary plate shape in the no-slip limit. Inversely, in the limit $b_0=b_1$ infinite, i.e., perfect slip, we obtain $p(x,y)=p_0$, $F_z^{\text{pressure}}=0$, and thus

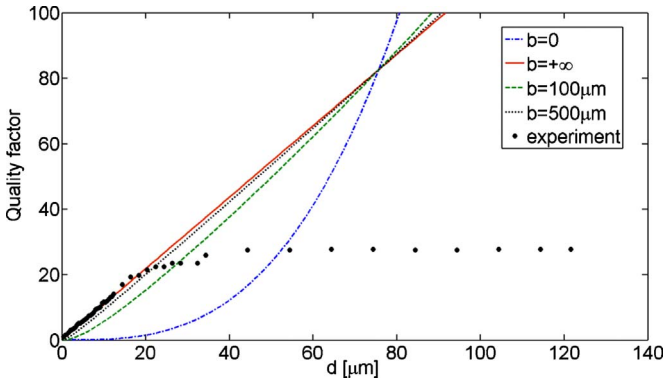

FIG. 2. (Color online) Evolution of the beam quality factor Q as a function of the gap d for different slip lengths b and for the lever mechanical properties given in Ref. [16]. The experimental data are in good agreement only with $b>500$ μm as shown on the red (continuous) curve.

$$F_z = -\frac{2\eta US}{d}, \tag{28}$$

which is the result used in Ref. [16] in the perfect-slip limit. It is worth noting that this formula is only dependent on the surface S of the vibrating plate and not on its exact geometry. It implies that the result obtained in Ref. [16] should be very robust with respect to geometry considerations. We point out that this perfect-slip limit can be directly obtained by solving the equation $\eta\partial_z^2 v_z=0$ with the boundary conditions for v_z. Indeed, the direct integration gives $v_z=Uz/d$. The pressure $p=p_0$ can be deduced similarly [25].

It is worth noting that in the derivation of all these formulas, the Reynolds assumption $\partial_z p=0$ implies also $\eta\partial_z^2 v_z=\partial_z p=0$. However, from Eq. (12), we deduce

$$\eta\partial_z^2 v_z = -\frac{A}{2}\left[z-\frac{2b_1+d}{b_0+b_1+d}\frac{d}{2}\right]. \tag{29}$$

In the perfect-slip limit (where $A\to 0$), the Reynolds condition is automatically fulfilled, i.e., the solution is self-consistent. However, in general, $\eta\partial_z^2 v_z \neq 0$ and this limits the validity of the previous results. The Reynolds hypothesis can nevertheless be justified, for all practical purposes, if $|\partial_z^2 v_z| \ll |\partial_z^2 v_i|$, that is, if $|z-\frac{2b_1+d}{b_0+b_1+d}\frac{d}{2}| \ll |\partial_i g|$. Since $|\partial_i g| \sim L$, where L is a typical lateral dimension of the lever, the Reynolds assumption is in general justified for $L \gg d$.

To study the influence of the slip length on the dynamic properties of the oscillator considered in Ref. [16], we will now consider a simplification. Such a simplified force expression is obtained if the condition $b_0=b_1=b$ is fulfilled. Considering, for example, the rectangular plate [in the limit given by Eq. (22)], we get for the total force

$$F_z = -\eta ULw\frac{L^2+12bd}{d^3+6bd^2}. \tag{30}$$

From this follows the damping constant $\gamma := -F_z/U$. To compare this result to the experiment, we show on Fig. 2 the evolution of the quality factor $Q=k/(\omega_0\gamma)$ of the oscillating beam calculated for a stiffness $k=0.0396$ N/m and a pulsation $\omega_0=2\pi\times 50$ kHz considered in Ref. [16] and for different slip lengths b. Clearly, the agreement with the experimental data is very good in the limit $d \lesssim \delta_B$ (i.e., far from the observed saturation at large gaps) for giant slip lengths such as $b>500$ μm (red curve). Oppositely, the reported results are in total conflict with the standard no-slip prediction $Q \sim d^3$ (blue curve). While the present study focused on the static regime, it is interesting to remark from dimensional analysis that one should expect to observe saturation around $\delta_B \simeq 10$ μm (i.e., $\gamma_{\lim}=2\eta S/\delta_B$). The value observed experimentally corresponds to $\delta_B \simeq 25$ μm, which is of the same order of magnitude but nevertheless significantly larger. The difference could be imputed to geometry considerations, i.e., to the fact that the dynamics of the fluid around the lever should be strongly influenced by the finite size of the system under study (indeed, in the regime where the boundary layer δ_B plays explicitly a role, retardation should be taken into account). A different explanation could be that the model of perfect slip breaks down at large gap. A preliminary analysis in that direction shows that if we conserve the inertial term in the Navier-Stokes equations, we indeed obtain a saturation regime due to an additional damping occurring on the length scale $b \sim \delta_B$ and this even if b is infinite in the static regime.

IV. DISCUSSION

Fundamentally, the existence of a giant slip length regime is very surprising and interesting and should therefore be discussed carefully. Here, we will only review some results which, we think, are important to justify microscopically the results discussed in this paper and in Ref. [16]. We remind that from a microscopic point of view, the slippage coefficient is actually linked to the very nature of the interaction between the oscillating surface and the air molecules. Historically, the first theoretical analysis of this phenomenon goes back to Maxwell and to its kinetic theory of gases [26]. Following this approach, one can indeed distinguish between a specular channel of interaction, for which the molecules are colliding elastically with the surface, and a channel of interaction for which molecules are reflected diffusively from the wall [9,21,26–30]. This second channel is linked to multiple collisions between molecules and also to adsorption by the surface. The slip length b in this statistical model is given by the Maxwell formula [21,26–30]

$$b \simeq \frac{2}{3}\bar{\lambda}\frac{2-p_d}{p_d}, \tag{31}$$

where $\bar{\lambda}$ is the typical mean-free path of gas molecules (i.e., $\bar{\lambda} \simeq 60$ nm for air in ambient conditions) and p_d the tangential momentum accommodation coefficient, i.e., the fraction of those molecules hitting the surface which are reflected diffusively. Clearly, if p_d vanishes, then the slip length is infinite. This suggests that in the working regime of our mechanical oscillator, the molecules are mainly reflected specularly. Furthermore, recent analysis based on the fluctuation dissipation theorem and the Green-Kubo relationship emphasizes the importance of several other microscopical parameters on the molecular dynamics close to a surface [9,22,23].

Altogether, these studies provide an estimate for the slip length given by

$$b \sim \frac{k_B T \eta D}{C_\perp \rho \sigma \epsilon^2}, \tag{32}$$

where D is the fluid diffusion coefficient, σ and ϵ are, respectively, a typical length and energy characterizing the molecular interaction, and $C_\perp$ a coefficient measuring the roughness (larger $C_\perp$ mean larger roughness). This shows the importance of surface roughness but also of surface defects and nanostructuration [23] for the physics of slippage at solid-gas interfaces. Future work should investigate the effects of theses parameters on the damping coefficient γ. It is worth noting that past studies on the slippage at a solid-fluid interface mainly focused on liquids for which the mean-free path is much smaller ($\bar{\lambda} \sim 1$ nm) and for which interactions between molecules are much stronger. The existence of a partial slip regime implies in those cases to work in the realm of nanofluidics (e.g., nanochannels) with separating gap d well below the micrometer range [7,22] or with AFMs in contact mode [22,31]. Here, oppositely, we consider gases and we can define a Knudsen coefficient $K_n = \bar{\lambda}/d \sim 0.001 - 0.06$ which corresponds to a regime of transition flow [7,9,23] occurring at large gap values d (it is indeed well known that important deviations to the no slip boundary conditions appear for $K_n \sim 10^{-3} - 10^{-2}$ [7]).

Another relevant length in the analysis is the vibration amplitude of the lever which we reported in Ref. [16] to be $\delta z \simeq 0.05$ nm. This is actually a very small amplitude which is attainable experimentally mainly because of the thermal excitation mode and high sensitivity of the optical detection setup used in [16]. This value for δz is also comparatively smaller that those attainable with actuated AFM [32]. Working in this regime where $\delta z/\bar{\lambda} \simeq 10^{-3} \ll 1$ could therefore lead to new physics and we expect that further studies in this direction will be done in a close future (e.g., to compare the effect of the vibration amplitude and of the excitation modes on the micro- and nanolever dynamics).

In this context, it is worth mentioning that the theoretical model developed in this paper for the plane-plane configuration constitutes the equivalent of the Vinogradova formula obtained for the sphere-plane configuration [9,17,18,23,32]. The analysis of Vinogradova generalizes the result obtained by Taylor [22] in the no-slip limit and which predicts a friction force $F_z = -6\pi\eta R^2 U/d$ for a sphere of radius R moving along the z axis with the velocity U perpendicularly to the interface $z=0$ and separated from this plane by a minimal gap d. It is interesting to point out that the no-slip condition predicts the same law $F_z \propto 1/d$ as in the plane-plane configuration with the perfect-slip condition [i.e., Eq. (28)] but with a different numerical value for $\gamma_{\text{Taylor}} := 6\pi\eta R^2/d$ [compare Eq. (1)]. The Vinogradova model predicts oppositely $F_z \simeq 2\pi\eta R^2 U \ln(6b/d)/b$ in the limit $b \to +\infty$ of the perfect slip. The different regimes of force depending of the value for the slippage length b and from the geometry considered are summarized in Table I.

The present problem reminds us of a very known similar difficulty encountered in experiments for measuring the Casimir force in the sphere-plane or plane-plane configuration. It is worth pointing out, however, that in the Casimir effect [33], the force in the plane-plane configuration varies as $F_z \sim \hbar S/d^4$ whereas it varies as $F_z \sim \hbar R/d^3$ for the sphere-plane configuration ($\hbar$ is the Planck constant). Besides the important difference in the power-law behavior in d between these expressions and those predicted by hydrodynamics, it is interesting to observe that in the perfect-slip limit, the viscous force decays slowly when d increases whereas the same force vanishes in the sphere-plane as predicted by the Vinogradova formula for $b=+\infty$. Therefore, in order to observe the perfect-slip regime, the plane-sphere configuration would be much more demanding than the plane-plane configuration studied in this work and in [16] since it implies that one should consider very small gaps d to obtain a finite effect with the sphere. This could have implication in optical near-field microscopy where viscosity is suggested as a possible mechanism to justify the shear force applied on the tip probes in high vacuum [34] (see also [35,36] for experimental demonstrations at cryogenic temperature). Additionally, this sensitivity of the force behavior with b in the sphere-plane configuration could be used to probe more precisely the value of the slippage length than in the plane-plane geometry. Oppositely, the giant slip effect studied in this paper could thus be a specificity of the planar geometry and is expected therefore to have a huge impact on the NEMS dynamics which are mostly developed with such geometry.

TABLE I. Table summarizing the asymptotic viscous force regimes for both the plane-plane and sphere-plane configurations and for the no-slip and perfect-slip cases.

	Plane-plane	Sphere-plane
$b=0$	$\gamma = -\eta\langle g\rangle S/d^3$	$\gamma = 6\pi\eta R^2/d$
$b \to +\infty$	$\gamma = 2\eta S/d$	$\gamma = 2\pi\eta R^2 \ln[d/(6b)]/b$

V. IMPLICATIONS FOR NEMS ARCHITECTURES AND DYNAMICS

This brings us to the second point that we shall now discuss in this section, which is the implication of our results for NEMS and MEMS engineering. Owing to the formula given by Eq. (1), the effect of dissipation on the beam motion decays very slowly with d and in particular we see that the quality factor $Q := m\omega_0/\gamma$ decreases linearly with d.

Additionally, when d decreases, the pulsation at resonance

$$\omega_{\text{reson.}} = \sqrt{\omega_0^2 - \frac{1}{2}\left(\frac{\gamma}{m}\right)^2} \tag{33}$$

is progressively downshifted [16]. This occurs until $\omega_{\text{reson.}} = 0$, i.e., from Eqs. (1) and (33) when the critical distance d_c given by

$$d_c = \frac{\sqrt{2}\eta L w}{m\omega_0} \tag{34}$$

is reached. For $d \leq d_c$, the lever motion is consequently overdamped (nonlinear effects are also expected in this limit). To

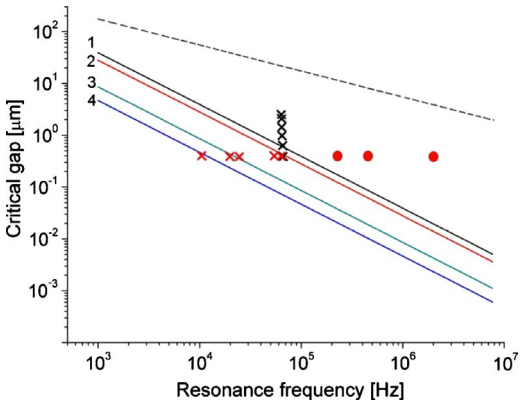

FIG. 3. (Color online) Evolution of critical gap as a function of frequency $f_0=\omega_0/(2\pi)$ for a Si (black line; numbered 1), SiC (red line; numbered 2), GaAs (green line; numbered 3), and Au (blue line; numbered 4) cantilever, respectively. Black dashed line corresponds to the limit associated with the boundary layer. Experimental data points for the lever studied in Ref. [16] at the internal resonance frequency 50 kHz are also shown for distance d close to the overdamping regime (black vertical crosses). Red (horizontal) crosses and circles correspond to characteristics of NEMS realized with a distance to the substrate constantly equal to $d=400$ nm. Such NEMS can approximately be modeled as the one shown in Fig. 1.

describe quantitatively the importance of such a regime on beam dynamics, we remind that for the levers considered here, we have $\omega_0=\sqrt{\frac{E}{12\rho}}r_0^2\frac{t}{L^2}$ and $m=\rho tLw$, where ρ is the bulk density, E is the Young's modulus, and $r_0\simeq 1.875$ 104 [37].

Figure 3 shows the variations of d_c as a function of $f_0=\omega_0/(2\pi)$ for a thin lever with $t=180$ nm (same as in Ref. [16]) and for different commonly used materials. For low frequencies in the 10 kHz range and below, the overdamping regime appears already at large separation distance $d_c\geq 0.1-1$ μm. Oppositely, for very high oscillator frequencies in the 100 kHz range and beyond, we have $d_c\lesssim 10-100$ nm and the overdamping regime becomes a fundamental issue only at the nanoscale. For comparison, we show on the same graph the experimental data points taken from Ref. [16] and corresponding to working distances d which are decreasing until the overdamped regime at d_c is reached. Additionally, we show also the physical characteristics recorded (i.e., internal resonance frequency f_0 and fixed distance gap $d=400$ nm with the substrate) of typical Si-made NEMS. These NEMSs can be with a good approximation described with the simple geometry considered here. Clearly, working with such NEMS in a gaseous environment may strongly affect their dynamics and only for very high f_0 could the overdamping regime actually be overcome. This is indeed confirmed for those NEMS annexed by a red cross in Fig. 3 which we studied experimentally by using the same optical method as described in Ref. [16]. The experiment showed that NEMSs with such gaps do not resonate in air at room temperature, confirming therefore the role played by overdamping. For the NEMS indicated by a red circle, i.e., with frequency in the 100 kHz and MHz ranges, we were out of the detection sensitivity of our setup and no data were available.

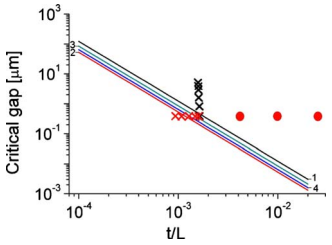

FIG. 4. (Color online) Evolution of the critical gap as a function of the ratio t/L for the same lever materials as in Fig. 3. Color lines numbering and data points have the same meaning as in Fig. 3.

As a complementary analysis, we show in Fig. 4 the explicit dependence of d_c on the aspect ratio t/L for different materials. In the typical range of aspect ratio considered, the overdamping regime covers distance gaps d going from the micrometer range to the nanoscale and, therefore, cannot be neglected. Again, this fact is confirmed by comparing these graphs to available experimental data (see Fig. 4 and compare to Fig. 3).

Furthermore, it is also useful to remind once again that for a large gap d, the important length scale is the boundary layer thickness δ_B which characterizes the spatial region surrounding the lever for which viscosity has an impact on the fluid dynamics [19,20]. For $d\geq\delta_B$, the substratum lies outside this layer and dissipation must saturate [19,20], as reported in Ref. [16]. Comparisons to values for d_c (see Fig. 3) show that the overdamping regime is always reached for gaps smaller than δ_B. The overdamping regime appears consequently as a robust limitation which should affect the design of any NEMS working in fluids. The results obtained here for a particular lever geometry are expected to be very general as soon as the beam geometrical dimensions are larger than δ_B. However, when dimensions are smaller, boundary effects due to the finite size of the system should explicitly be taken into account in the definition of d_c.

VI. CONCLUSION

In this paper, we studied the linearized Navier-Stokes equation in the static regime to describe the damping mechanism of oscillating microplates in air close to a substrate. We considered the influence of the slip length and showed that results reported in Ref. [16] are only compatible with very large slip length in the range $b>500$ μm. We discussed the implication of this mechanism on the oscillation properties of NEMS and showed that an overdamping behavior represents a fundamental mechanism for such systems. We expect that this work could have important consequences for NEMS engineering.

ACKNOWLEDGMENT

This research was partly supported by a "Carnot-NEMS" collaborative grant between CEA-LETI and Institut Néel.

APPENDIX: THE RECTANGULAR PLATE IN THE STATIC REGIME

The aim of this appendix is to solve the Poisson equation $(\partial_x^2+\partial_y^2)p(x,y)=A$, where A is a constant for the rectangular

domain $L \times w$ with boundary conditions $p=p_0$ along the contour. Using a Fourier series satisfying these boundary conditions at $x=0$ and $x=L$, we can write

$$p(x,y) = p_0 + \sum_n c_n(y) \sin\left(\frac{\pi n x}{L}\right). \tag{A1}$$

Here, $c_n(y)$ is solution of

$$-\left(\frac{\pi n}{L}\right)^2 c_n(y) + \frac{d^2}{dy^2} c_n(y) = \frac{4A}{n\pi} \epsilon_n, \tag{A2}$$

with $\epsilon_n=1$ if n is an odd integer and $\epsilon_n=0$ if n is even. The general solution of this equation is

$$c_n(y) = a_n^{(+)} e^{+\pi n y/L} + a_n^{(-)} e^{-\pi n y/L} - \frac{4A}{n^3\pi^3} L^2 \epsilon_n. \tag{A3}$$

The constant $a_n^{(\pm)}$ are determined by the boundary conditions $p=p_0$ at $y=0$ and $y=w$. One therefore obtains

$$a_n^{(-)} = \frac{4A}{n^3\pi^3} L^2 \epsilon_n \frac{[e^{+\pi n w/L} - 1]}{[e^{+\pi n w/L} - e^{-\pi n w/L}]},$$

$$a_n^{(+)} = \frac{4A}{n^3\pi^3} L^2 \epsilon_n \frac{[1 - e^{-\pi n w/L}]}{[e^{+\pi n w/L} - e^{-\pi n w/L}]}. \tag{A4}$$

This leads to

$$p(x,y) = p_0 + \frac{4AL^2}{\pi^3} \sum_n \frac{\epsilon_n}{n^3} \sin(\pi n x/L) \times \left[-1 + \frac{1 - e^{-\pi n w/L}}{e^{+\pi n w/L} - e^{-\pi n w/L}} e^{+\pi n y/L} + \frac{e^{+\pi n w/L} - 1}{e^{+\pi n w/L} - e^{-\pi n w/L}} e^{-\pi n y/L} \right]. \tag{A5}$$

[1] M. Li, H. X. Tang, and M. L. Roukes, Nat. Nanotechnol. **2**, 114 (2007).
[2] C. Metzger, M. Ludwig, C. Neuenhahn, A. Ortlieb, I. Favero, K. Karrai, and F. Marquardt, Phys. Rev. Lett. **101**, 133903 (2008); G. Jourdan, F. Comin, and J. Chevrier, *ibid.* **101**, 133904 (2008).
[3] Y. T. Yang *et al.*, Nano Lett. **6**, 583 (2006).
[4] K. L. Ekinci, Y. T. Yang, and M. L. Roukes, J. Appl. Phys. **95**, 2682 (2004).
[5] J. N. Munday, F. Capasso, and A. Parsegian, Nature (London) **457**, 170 (2009).
[6] H. J. Mamin and D. Rugar, Appl. Phys. Lett. **79**, 3358 (2001).
[7] P. Tabeling, *Introduction to Microfluidics* (Oxford University Press, USA, 2006).
[8] P. Joseph, C. Cottin-Bizonne, J.-M. Benoît, C. Ybert, C. Journet, P. Tabeling, and L. Bocquet, Phys. Rev. Lett. **97**, 156104 (2006).
[9] E. Lauga, in *Handbook of Experimental Fluid Dynamics*, edited by J. Foss, C. Tropea, and A. Yarin (Springer, New York, 2007), Chap. 19, p. 1219.
[10] C. P. Green and J. E. Sader, J. Appl. Phys. **98**, 114913 (2005).
[11] T. Naik, E. K. Longmire, and S. C. Mantell, Sens. Actuators, A **102**, 240 (2003).
[12] M. R. Paul and M. C. Cross, Phys. Rev. Lett. **92**, 235501 (2004).
[13] J. Dorignac, A. Kalinowski, S. Erramilli, and P. Mohanty, Phys. Rev. Lett. **96**, 186105 (2006).
[14] S. Basak, A. Raman, and S. V. Garimella, J. Appl. Phys. **99**, 114906 (2006).
[15] R. C. Tung, A. Jana, and A. Raman, J. Appl. Phys. **104**, 114905 (2008).
[16] A. Siria, A. Drezet, F. Marchi, F. Comin, S. Huant, and J. Chevrier, Phys. Rev. Lett. **102**, 254503 (2009).
[17] O. I. Vinogradova, Langmuir **11**, 2213 (1995).
[18] O. I. Vinogradova, Langmuir **14**, 2827 (1998).
[19] L. D. Landau and E. M. Lifshitz, *Fluid Mechanics* (Pergamon, Oxford, 1975).
[20] G. K. Batchelor, *Fluid Dynamics* (Cambridge University Press, Cambridge, England, 1974).
[21] L. B. Loeb, *The Kinetic Theory of Gases* (McGraw-Hill, New York, 1927).
[22] C. Neto *et al.*, Rep. Prog. Phys. **68**, 2859 (2005).
[23] L. Bocquet and E. Charlaix, Chem. Soc. Rev. **39**, 1073 (2010).
[24] C. L. M. H. Navier, Mémoire de l'Académie Royale des Sciences de l'Institut de France **6**, 389 (1823).
[25] The pressure can be deduced from the equation $\nabla^2 p=0$ which results from the Navier-Stokes equation [19,20]. Supposing $\partial_z p=0$ leads to $(\partial_x^2+\partial_y^2)p=0$. Applying the boundary condition $p=p_0$ along the contour together with the uniqueness theorem implies directly $p=p_0$ everywhere. Finally, it is worth noting that the solutions of the Navier-Stokes equations $\partial_z^2 v_i=0$ $(i=x,y)$ are $v_i(x,y,z)=\alpha_i(x,y)z+\beta_i(x,y)$. The perfect-slip boundary conditions then lead to $\alpha_i=0$ and the imcompressibility relation to $\partial_x\beta_x+\partial_y\beta_y=-U/d$.
[26] J. C. Maxwell, Philos. Trans. R. Soc. London, Ser. B **170**, 231 (1879).
[27] M. Fichman and G. Hetsroni, Phys. Fluids **17**, 123102 (2005).
[28] G. Arya *et al.*, Mol. Simul. **29**, 697 (2003).
[29] Z. L. Guo *et al.*, Europhys. Lett. **80**, 24001 (2007).
[30] F. Sharipov and D. Kalempa, Phys. Fluids **15**, 1800 (2003).
[31] A. Maali, T. Cohen-Bouhacina, G. Couturier, and J. P. Aime, Phys. Rev. Lett. **96**, 086105 (2006).
[32] A. Maali and B. Bhushan, Phys. Rev. E **78**, 027302 (2008).
[33] C. Genet *et al.*, Ann. Fond. Louis Broglie **29**, 331 (2004).
[34] K. Karrai and I. Tiemann, Phys. Rev. B **62**, 13174 (2000).
[35] M. Brun *et al.*, J. Microsc. **202**, 202 (2001).
[36] M. Brun *et al.*, Europhys. Lett. **64**, 634 (2003).
[37] A. N. Cleland, *Foundation of Nanomechanics* (Springer-Verlag, Germany, 2004).